Genomics Proteomics Bioinformatics 21 (2023) 1030–1042

Genomics Proteomics Bioinformatics

www.elsevier.com/locate/gpb
www.sciencedirect.com

ORIGINAL RESEARCH

MicroRNA–disease Network Analysis Repurposes Methotrexate for the Treatment of Abdominal Aortic Aneurysm in Mice

Yicong Shen [1,#], Yuanxu Gao [1,2,3,#], Jiangcheng Shi [1,3], Zhou Huang [1,3], Rongbo Dai [1], Yi Fu [1], Yuan Zhou [1,3], Wei Kong [1,*], Qinghua Cui [1,3,*]

[1] *Department of Physiology and Pathophysiology, School of Basic Medical Sciences, State Key Laboratory of Vascular Homeostasis and Remodeling, Peking University, Beijing 100191, China*
[2] *State Key Laboratory of Lunar and Planetary Sciences, Macau University of Science and Technology, Macao Special Administrative Region 999078, China*
[3] *Department of Biomedical Informatics, Center for Noncoding RNA Medicine, School of Basic Medical Sciences, Peking University, Beijing 100191, China*

Received 24 September 2021; revised 15 July 2022; accepted 19 August 2022
Available online 24 August 2022

Handled by Edwin Wang

KEYWORDS

Abdominal aortic aneurysm;
Network medicine;
MicroRNA-derived disease network;
Autoimmune disease;
Methotrexate

Abstract **Abdominal aortic aneurysm** (AAA) is a permanent dilatation of the abdominal aorta and is highly lethal. The main purpose of the current study is to search for noninvasive medical therapies for AAA, for which there is currently no effective drug therapy. **Network medicine** represents a cutting-edge technology, as analysis and modeling of disease networks can provide critical clues regarding the etiology of specific diseases and therapeutics that may be effective. Here, we proposed a novel algorithm to quantify disease relations based on a large accumulated microRNA–disease association dataset and then built a disease network covering 15 disease classes and 304 diseases. Analysis revealed some patterns for these diseases. For instance, diseases tended to be clustered and coherent in the network. Surprisingly, we found that AAA showed the strongest similarity with rheumatoid arthritis and systemic lupus erythematosus, both of which are **autoimmune diseases**, suggesting that AAA could be one type of autoimmune diseases in etiology. Based on this observation, we further hypothesized that drugs for autoimmune diseases could be repurposed for the prevention and therapy of AAA. Finally, animal experiments confirmed that **methotrexate**, a drug for autoimmune diseases, was able to alleviate the formation and development of AAA.

* Corresponding authors.
E-mail: cuiqinghua@bjmu.edu.cn (Cui Q), kongw@bjmu.edu.cn (Kong W).
# Equal contributions.

Peer review under responsibility of Beijing Institute of Genomics, Chinese Academy of Sciences / China National Center for Bioinformation and Genetics Society of China.

https://doi.org/10.1016/j.gpb.2022.08.002

Introduction

Abdominal aortic aneurysm (AAA) is a cardiovascular disorder describing a permanent, thick, localized dilatation of the abdominal aorta, which commonly affects the infrarenal part [1,2]. AAA is diagnosed if an abdominal aorta exceeds the normal vessel diameter by 50% or the diameter of the abdominal aorta is greater than 30 mm [3,4]. The global prevalence rate of AAA per 100,000 people ranges from over 1000 in the 65-to-69-year-old group to approximately 3000 in people over 80 years old [5]. The main complication of AAA is aortic rupture, before which AAA is usually asymptomatic. AAA rupture has a mortality rate of 85%–90% and is estimated to cause 150,000–200,000 deaths each year worldwide [6]. Currently, the usual treatment for large or symptomatic AAAs is open surgery or endovascular repair [2,7]. However, early elective surgical repair of small AAAs does not provide a significant benefit, and there is still no drug recommended for the effective prevention of AAA enlargement and rupture. Although many potential therapeutic targets for AAA have been identified and several clinical trials of the relevant drugs are already completed, the results showed these agents to be ineffective, including doxycycline, pemirolast, propranolol, amlodipine, and fenofibrate [2]. Thus, noninvasive medical therapies for AAAs to limit aneurysm expansion and prevent rupture are urgently needed.

Due to the time and economic resources involved in developing new drugs, we are attempting to use the strategy of drug repurposing (also known as drug repositioning) to find drug therapies for AAA. Drug repurposing is an emerging drug development strategy that applies approved or investigational drugs to new diseases or indications that are different from the original medical application [8]. In recent years, drug repurposing has received increasing attention from researchers due to its reduced risk of failure, shortened research and development cycle, and reduced cost compared with new drug development [9,10].

Network analysis is one of the approaches used in drug repurposing. In recent years, thanks to the accumulation of biomedical datasets and the improvement of artificial intelligence (AI), network medicine has emerged as a cutting-edge conceptual framework for clinical and basic medical research [11,12]. Network medicine greatly speeds up progress toward precision medicine, including the prediction of gene functions, gene–disease associations, drug repurposing, and the discovery of disease modules [13]. For example, analysis and modeling of patient or disease networks built according to some similarity metric is an excellent strategy to interpret the nature of specific diseases [14] and discover disease subtypes [15]. Historically, disease networks have been built using various biomedical data and similarity metrics [16,17], and different data types have made specific contributions to clarifying the complex relationships among diseases. It is crucial to use disease networks to guide drug repurposing strategies.

MicroRNAs (miRNAs) are a class of small non-coding RNAs that perform important functions at the post-transcriptional level [18]. miRNA dysfunctions could be associated with many human diseases, including cancer and cardiovascular diseases [19]. A given disease, especially a complex disease, is usually related to some other diseases in the sense that their underlying mechanisms have certain genes and pathways in common [20]. Thus, systematic and quantitative methods, such as network analysis, play increasingly important roles in the analysis of complex diseases [20–22]. In the last decade, many such studies have been performed [16,17,23]. We previously analyzed human miRNA–disease association data using a network biology approach [24]. However, that study had two major limitations. First, the data on miRNA–disease associations were quite limited ten years ago, when the research took place. Second, the network model and bipartite graph, used in that study do not define the direction (positive/negative) and the weight of disease relations. Recently, we updated the human microRNA disease database (HMDD) [19] with more comprehensive association data and more accurate classification, which made it possible for us to dissect complex diseases with more sophisticated mathematical tools. Based on these findings, network analysis using data on miRNA–disease associations may aid in identifying targets for repurposed drugs to help us discover drug therapies for AAA.

Here, we first collected and curated miRNA–disease associations with expression information from our HMDD database. Then we developed a proposed algorithm to quantify the similarity between any two diseases in the dataset. Next, we built a novel miRNA-based disease network (MRDN) based on the calculated disease similarity values and identified a number of patterns using a network biology approach. Moreover, we found that AAA is highly similar to autoimmune diseases but not to other cardiovascular diseases. This finding thus suggests the repurposing of methotrexate (MTX), a popular drug for autoimmune diseases, into an agent for the prevention and therapy of AAA. Finally, animal experiments confirmed the predicted effectiveness of MTX for this purpose.

Results

Curation of the human miRNA–disease association dataset

The workflow of this study is shown in **Figure 1**, which including network analysis and drug repurposing. To construct the disease network, a total of 5103 entries that recorded miRNA tissue expression regulation information were collected from the HMDD, accounting for 15.8% of all entries. As a result, 3357 unique miRNA–disease association pairs were classified, including 1788 up-regulated pairs and 1569 down-regulated pairs. All diseases were classified into 15 categories according to the Medical Subject Headings (MeSH) category tree. Neoplasms, cardiovascular diseases, and nervous system diseases were the top 3 most frequent disease classes (**Figure 2**A). The top 10 diseases with the highest numbers of associated miRNAs are shown in Figure 2B. Nine of them were neoplasms, and the disease with the largest number of miRNAs was hepatocellular carcinoma, in which 171 miRNAs were altered in expression. The top 10 miRNAs with the highest numbers of associated diseases are shown in Figure 2C. All these miRNAs were associated with at least 17 neoplasm diseases and at least 1 cardiovascular disease (Table S1).

Overview of the diseases and miRNAs in MRDN

To quantitatively analyze the relationships between diseases, we characterized each disease using its own miRNA-based

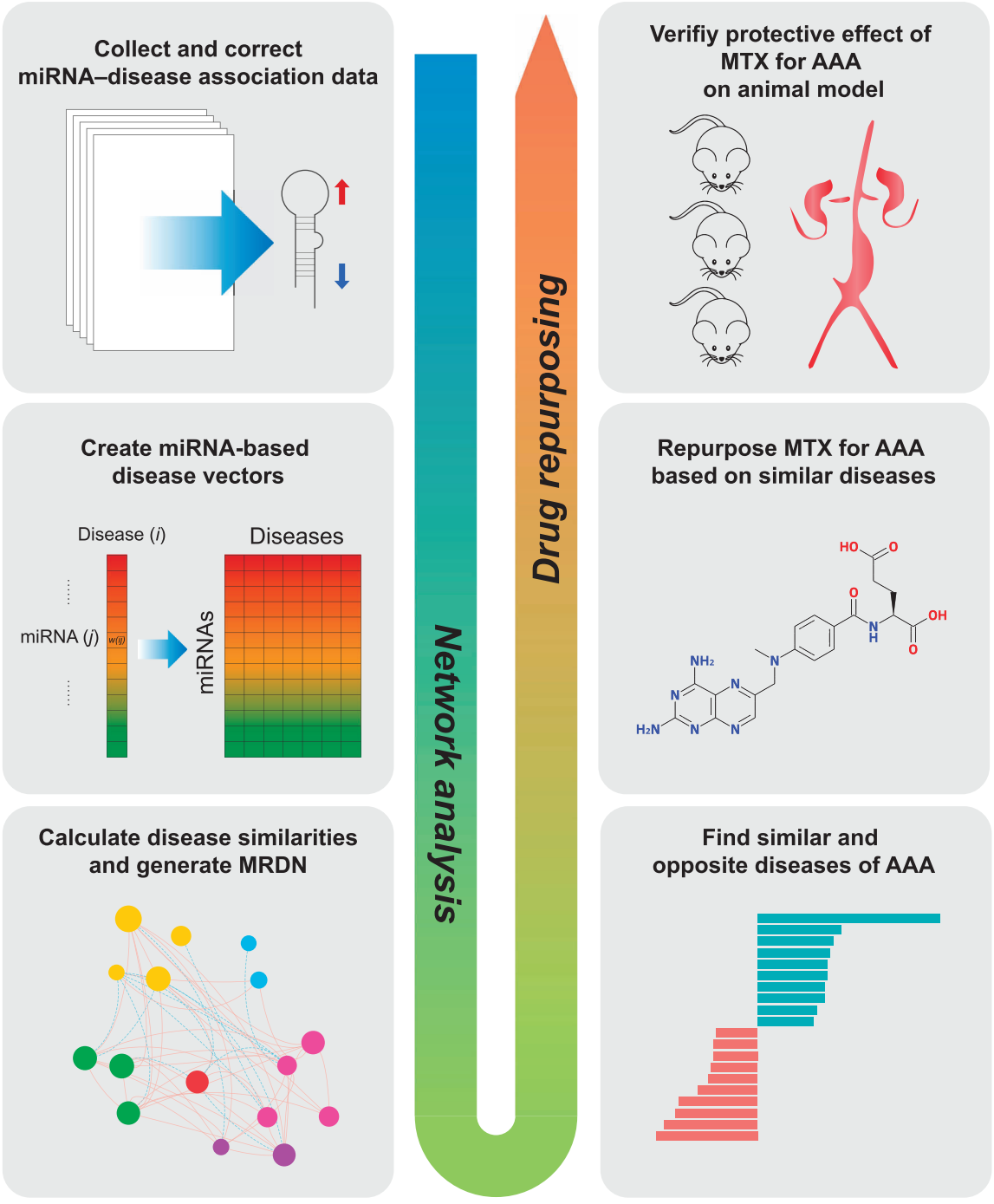

Figure 1 Overview of workflow
miRNA, microRNA; MTX, methotrexate; MRDN, miRNA-based disease network; AAA, abdominal aortic aneurysm.

vector (see details in Materials and methods). All disease vectors were then organized into a weight matrix, in which each row represents one miRNA and each column represents one disease (Figure S1; Table S2). In the weight matrix heatmap, most cancers are clustered and gathered on one side. Many diseases associated with few miRNAs are gathered on the other side. Then, we calculated pairwise disease similarities based on the disease vectors and constructed the MRDN based on the calculated disease similarities. Any two diseases had a nonzero similarity if they shared at least one miRNA, and the similarity was very close to zero if the number of shared miRNAs was much lower than the number of associated miRNAs. Thus, an MRDN constructed by assigning an edge to every pair of diseases with nonzero similarity would be extremely dense and almost fully connected, which might cause some difficulties in subsequent analysis. For example, network distance, which is normally a useful metric in network analysis, would be unhelpful because the network distance between any two nodes in a fully connected network is 1. To avoid the aforementioned situation, we empirically selected a similar-

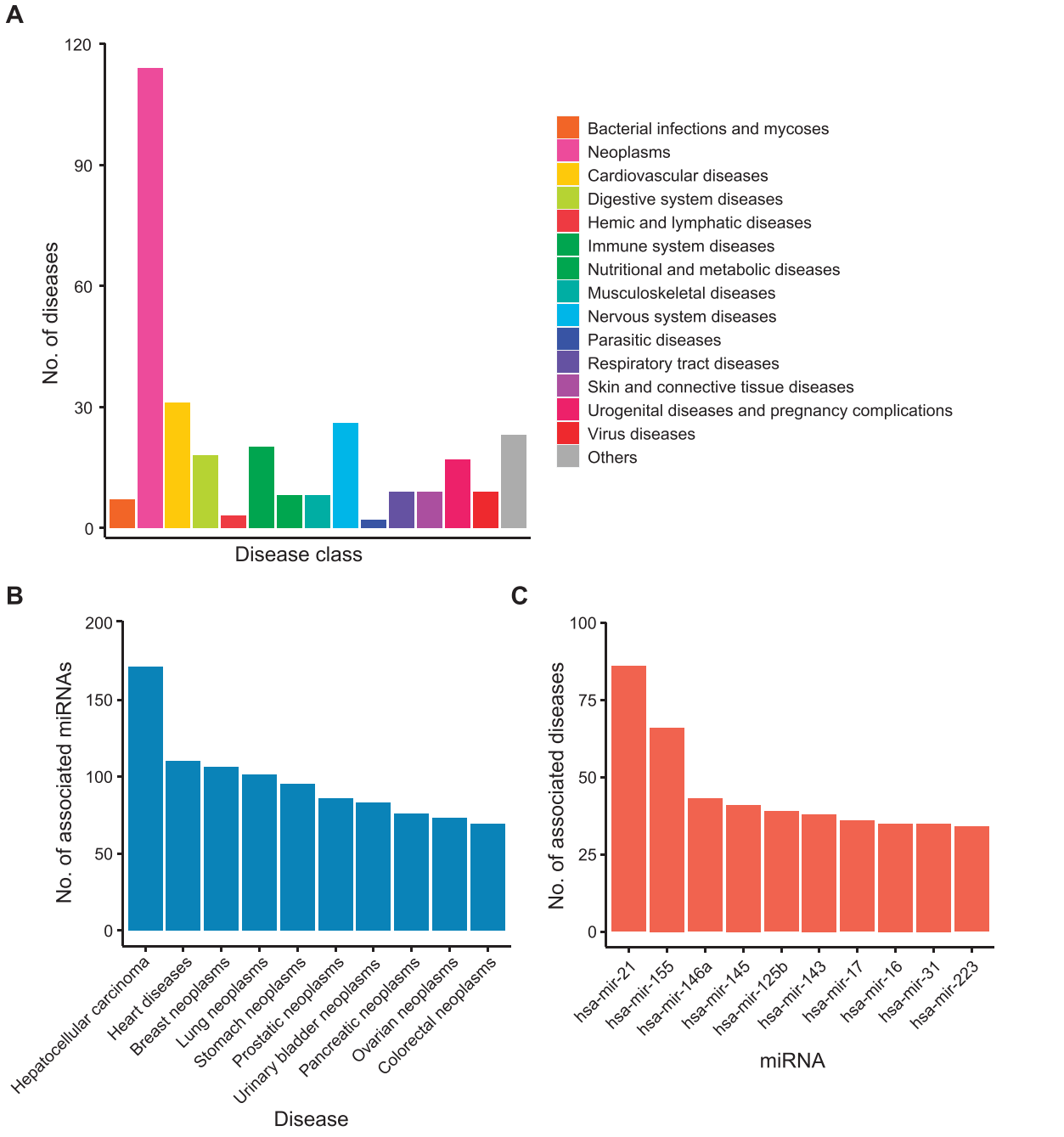

Figure 2 Overview of the human miRNA–disease association dataset

A. The number of diseases in different disease classes. **B.** The top 10 diseases with the highest numbers of associated miRNAs. **C.** The top 10 miRNAs with the highest numbers of associated diseases.

ity threshold of ± 0.05 to generate our human disease network. Any two diseases whose similarity was above 0.05 or below -0.05 were connected, and the resulting edges were defined as positive and negative, respectively. As a result, we obtained a MRDN with 304 nodes (diseases) and 2440 edges, which included 1521 positive edges and 919 negative edges (**Figure 3**A). The MRDN consisted of a giant interconnected component and 7 isolated nodes, suggesting that most diseases were more or less associated with each other at the miRNA level. The distributions of node degrees, cluster coefficients, miRNA weights, and disease similarities are shown in Figure S2. In the network, each disease is connected to ~ 16 other diseases on average, with 10 similar diseases and 6 opposite diseases. Moreover, we found that the number of positive edges was highly correlated with the number of negative edges ($R = 0.44$, $P = 7.39\text{E}{-16}$) (Figure 3B), indicating that diseases with a greater number of similar diseases tend to have a greater number of opposite diseases as well. On the other hand, several diseases, such as myelodysplastic syndromes, hypertrophic cardiomyopathy, and Alzheimer's disease, tend

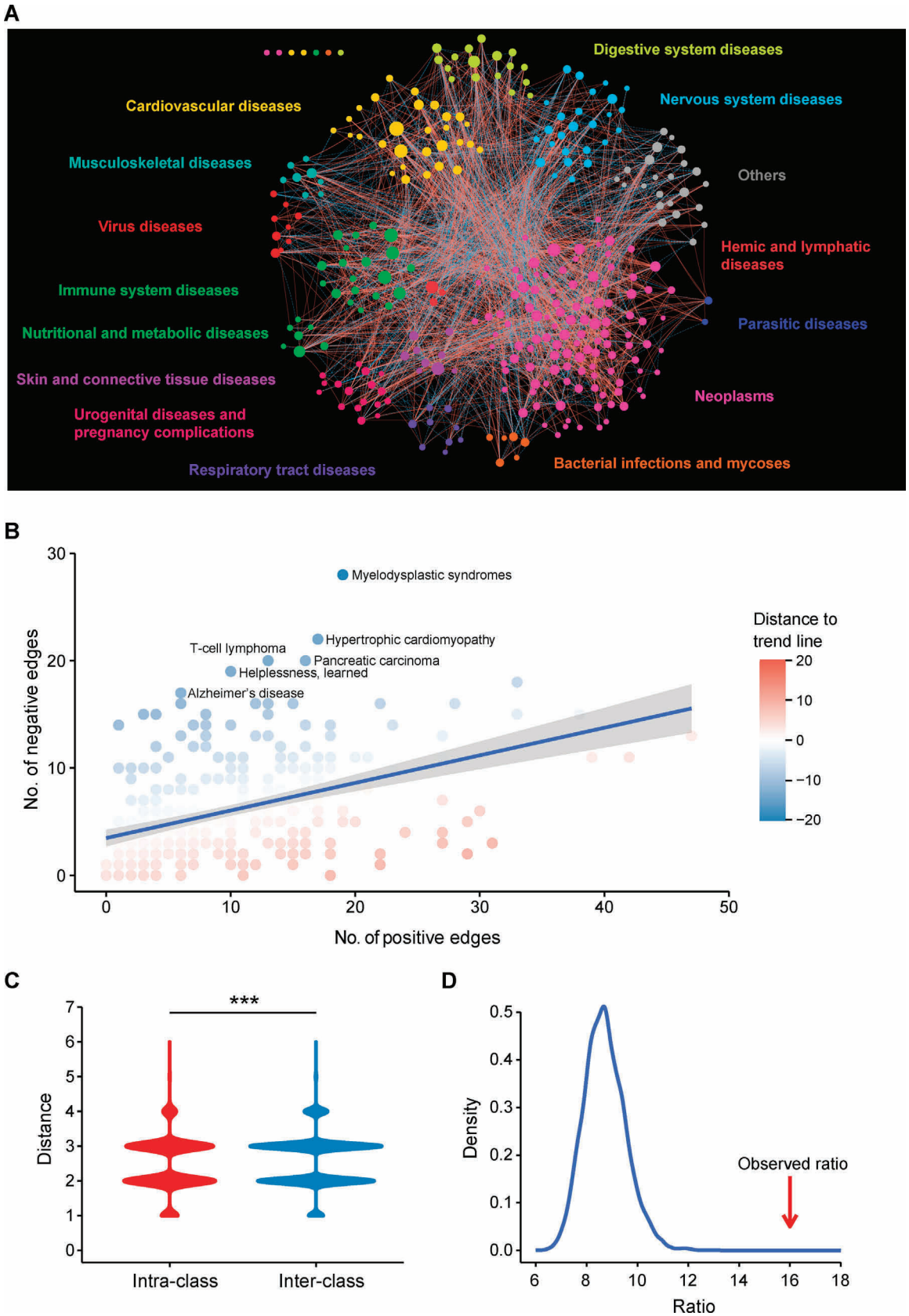

Figure 3 Network properties of MRDN

A. Overview of MRDN. In this network, each node represents one disease and the size of the node represents degree. The red solid lines or the blue dotted lines represent positive or negative edges between two diseases, respectively. **B.** The number of the positive edges is significantly correlated with the number of the negative edges of nodes ($R = 0.44$, $P = 7.39-E16$, Pearson correlation analysis). **C.** Diseases are clustered in MRDN. Distances within disease classes are significantly shorter than those between disease classes (Student's *t*-test, $P = 5.13E-31$). **D.** Disease loops in MRDN are coherent. Distribution of ratios of coherent to incoherent 3-cliques in randomization test. The observed ratio in MRDN is significantly higher than the random ones ($P < 0.0001$, randomization test).

to share more opposite diseases but fewer similar diseases. The identity of these diseases might result from their distinct pathogenesis compared to cancers, as a majority of diseases in our dataset were neoplasms [25–27].

Diseases in MRDN tend to be clustered and coherent

Diseases showed clustered architecture in the MRDN

We first investigated the network distance between diseases from the same MeSH class and different MeSH classes in the MRDN. Network distance, defined as the length of the shortest path between two nodes in the network, represents the closeness of two diseases. Here, we calculated the pairwise network distances of diseases in the MRDN and classified them into interclass distance and intraclass distance, defined as the distances between two diseases from the same class and different classes, respectively. The results showed that diseases from the same class were separated by a shorter distance than those from different classes (Figure 3C, Student's *t*-test, $P = 5.13E{-}31$), suggesting that diseases from the same MeSH classes tend to be close in the MRDN.

We further investigated the patterns of miRNA dysfunctions between diseases within the same classes and between different classes in terms of the numbers of positive edges and negative edges between them. We found that diseases from the same class are more likely than those from different classes to be linked in the MRDN (Table S3, Fisher's exact test, $P = 1.02E{-}20$), suggesting that diseases from the same class have more associations with each other at the miRNA level. In addition, diseases within the same class are more linked by positive edges instead of negative edges (**Table 1**, Fisher's exact test, $P = 6.59E{-}07$), suggesting that diseases within the same class tend to share the same pattern of miRNA dysfunction compared with diseases in different classes. Moreover, pairwise Fisher's exact tests were performed on disease classes, and the results showed that cancers and nervous system diseases tended to have opposite miRNA dysfunction patterns (**Table 2**, Fisher's exact test, $P = 1.97E{-}04$).

Disease loops are coherent

The relationships between diseases are thought to be consistent among themselves. For example, given diseases A and B, if they are both similar to disease C, it is expected that disease A and disease B are also similar, which is reflected in the network by three positive edges connecting the three nodes [16]. This property can be taken as a definition for coherence of disease loops in the MRDN. To investigate the coherence of edges between a set of connected diseases, we explored the edge signs of 3-cliques, that is, three-node disease loops, in the MRDN. We categorize the 3-cliques into two types based on the signs of their edges. One type is a coherent loop, which is described as a 3-clique with an even number (0 or 2) of negative edges; the other is an incoherent loop, which is described as a 3-clique with an odd number (1 or 3) of negative edges. It is speculated that coherent loops should be more plentiful in number and proportion than incoherent loops in the MRDN.

To confirm our hypothesis, we calculated the numbers of four types of 3-cliques in the MRDN using mfinder [28]. We obtained a total of 6024 3-cliques, comprising 5670 coherent 3-cliques and only 354 incoherent 3-cliques (coherent *vs*. incoherent: $\sim$ 16:1). To verify whether the disease loops tend to be coherent, we performed a randomization test by shuffling miRNAs and diseases 10,000 times. Then, we recalculated the pairwise disease similarity and reconstructed the MRDN in each round. The number and the ratio of coherent 3-cliques were also recalculated using mfinder. As a result, the expected number of coherent 3-cliques in the randomization test was 1378, and the expected ratio of coherent to incoherent 3-cliques was 8.72 (Figure 3D). The previously observed ratio in the real MRDN was 16.02, suggesting that the disease loops in the MRDN tended to be coherent ($P < 1E{-}200$).

Table 1 The similarity pattern of diseases within same classes and between different classes

	Intra-class	Inter-class
No. of positive links	432	1089
No. of negative links	179	740
Fisher's exact test	$P = 6.59E{-}07$	

Table 2 The similarity pattern of diseases within and between neoplasms and nervous system diseases

	Neoplasms	Nervous system diseases	Intra-class	Inter-class
No. of positive links	273	9	282	48
No. of negative links	94	6	100	43
Fisher's exact test	–	–	$P = 1.97E{-}04$	

MTX alleviated the formation and development of AAA

To discover novel disease relationships, we investigated the components of neighboring diseases' categories (Table S4). We found that approximately one-third of diseases (112 total) belonged to the disease category that was most frequent among their neighbors, which is consistent with our empirical knowledge that diseases from the same category tend to be associated with each other. Neoplasms are the most frequent category of neighbors to other diseases, including cardiovascular diseases. However, the most frequent category of neighbors to AAA is immune system diseases (7/28), which is an interesting finding that merits further investigation. To further validate the nonrandom nature of our observations, we performed a degree-preserving permutation test (Figure S3). The number of immune system diseases among the neighbors of AAA was significantly higher in the MRDN than in random networks (Student's *t*-test, $P < 1E{-}200$), indicating that the association between AAA and immune diseases is reliable.

AAA rupture is often lethal, with $\sim$ 90% mortality. Currently, open surgery and endovascular repair are the most effective interventions for large AAAs; however, there are still no drugs to treat AAA. Therefore, the discovery of drugs to treat AAA is one of the most important projects in AAA research. This study is the first to quantify the similarity of AAA with other diseases using a dataset of associations between miRNAs and diseases. We found that AAA was linked with 28 diseases in the MRDN through 6 miRNAs (**Figure 4**A; Table S5). Surprisingly, AAA was most similar to two autoimmune diseases, namely, rheumatoid arthritis (RA) and systemic lupus erythematosus (SLE), rather than

other cardiovascular diseases (Figure 4B), which suggests that AAA and autoimmune diseases might share part of their pathogenesis. This finding also supports the "Decline of the atherogenic theory of the etiology of the AAA and rise of the autoimmune hypothesis" [29]. We also investigated the 6 miRNAs that linked AAA and autoimmune diseases. These miRNAs were involved in 112 diseases across 14 categories, among which neoplasms and immune system diseases were the most represented categories. These results further suggest that drugs for autoimmune diseases could be repurposed for AAA. Given the aforementioned hypothesis, we reviewed the clinical guides for RA and SLE [30,31] and chose two drugs, namely, MTX and hydroxychloroquine (HCQ), which are immunosuppressants widely applied in autoimmune diseases, as potential drugs for AAA.

To validate the aforementioned prediction, we evaluated the potential effect of MTX on elastase-induced AAA. Mice were administrated with MTX (15 mg/kg, twice a week) [32] by oral gavage during 2 weeks of elastase induction (**Figure 5**A). As results, MTX administration significantly attenuated the elastase-induced expansion of the infrarenal aorta (Figure 5B and C) and the degradation of elastin (Figure 5D and E) compared with saline treatment. Moreover, the infiltration of macrophages in the aneurysmal wall was also markedly decreased following oral gavage with MTX (Figure 5F). These results indicated that MTX markedly mitigated vascular inflammation and AAA formation.

We next explored the possible effect of MTX on existing AAAs; MTX was administered to mice by oral gavage twice a week at a dose of 15 mg/kg or 25 mg/kg for an additional 2 weeks following the 2-week induction of AAA (**Figure 6**A, Figure S4A). Consequently, no significant alterations were observed in elastase-induced AAA at a dose of 15 mg/kg (Figure S4B and C). However, MTX at a 25 mg/kg dose obviously retarded the infrarenal aorta expansion and macrophage infiltration, although no significant alterations on elastin degradation, implying that a 25 mg/kg dose of MTX may display a potential therapeutic effect on AAA development by alleviating inflammation (Figure 6B–F).

In addition, we investigated the latent effect of HCQ on elastase-induced AAA. The mice received oral gavage of HCQ (100 mg/kg, daily) [33] (Figure S5A). The results showed that HCQ administration did not attenuate the development of AAA (Figure S5B and C).

Discussion

AAA rupture is often lethal, with ~ 90% mortality. Currently, open surgery and endovascular repair are recognized as effective interventions for large AAAs; however, there are not currently any drugs for AAA treatment [2]. In the current study, we found that AAA was most similar to autoimmune diseases, based on the construction of a MRDN. MTX, a conventional disease-modifying anti-rheumatic drug (DMARD) used for first-line treatment of RA and SLE, could be repurposed as a new treatment for AAA based on disease similarity. Based on the present study, it is plausible that MTX holds great promise for preventing the formation and development of AAA.

Over the past two decades, network medicine has greatly contributed to exploring and understanding complex biological systems [34]. Using a network-based approach to analyze diseases could not only provide a global view to discern general patterns and principles of human diseases but also help to characterize disease etiologies and discover therapy targets. Here, we curated the human miRNA–disease association dataset from our HMDD database and performed a comprehensive analysis of the data using the framework of network medicine. We found that human diseases were clustered and coherent in the MRDN. More importantly, we found that AAA was most similar to two autoimmune diseases, RA and SLE, rather than other cardiovascular diseases. The idea that AAA has characteristics of autoimmune disease was proposed over twenty years ago [35]. Human leukocyte antigen (HLA) levels, which play a key role in the presentation of self-proteins as observed in RA, are significantly different between AAA patients and non-AAA patients [36]. However, there was still insufficient evidence that AAA is an autoimmune disease.

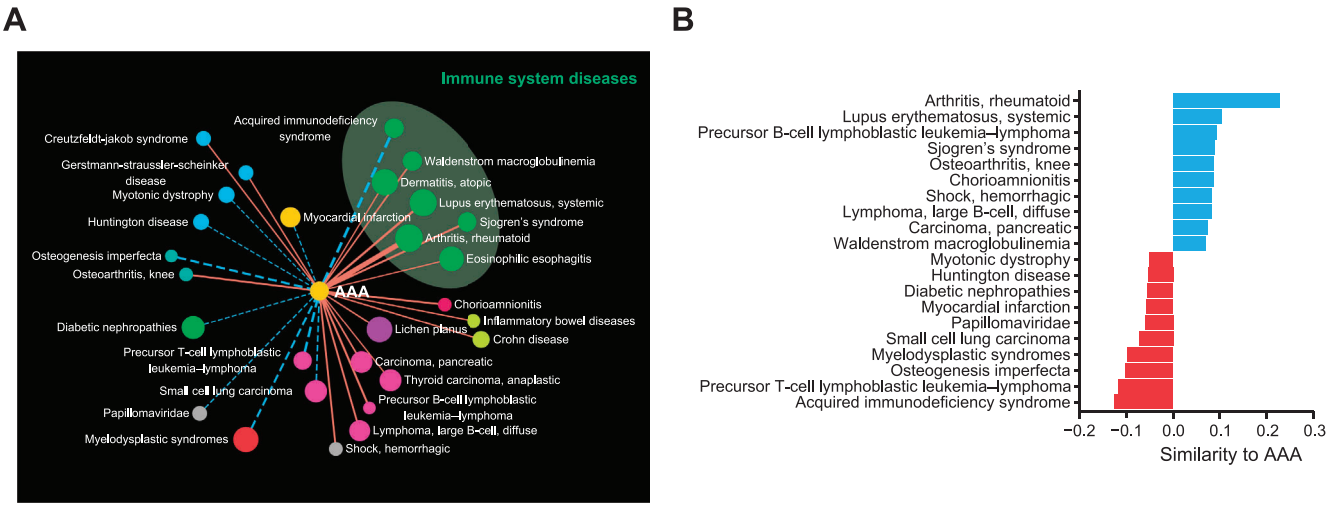

Figure 4 Repurposing MTX for the treatment of AAA

A. First neighbor diseases of AAA in MRDN. The subnetwork includes 29 nodes with 18 positive edges and 10 negative edges. **B.** Similarities of the top 10 similar and the top 10 opposite diseases of AAA.

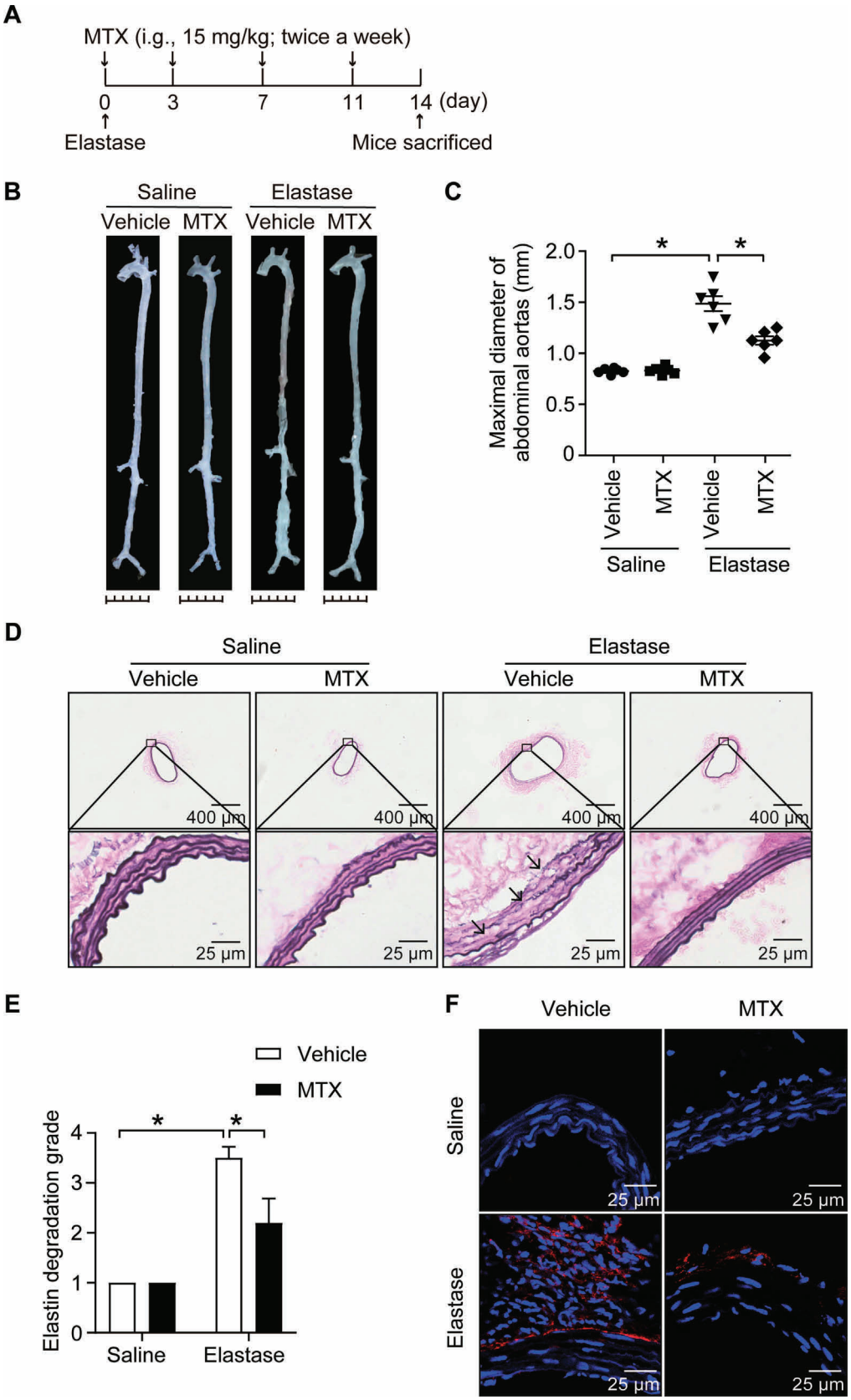
A
MTX (i.g., 15 mg/kg; twice a week)
0
3
7
11
14 (day)
Elastase
Mice sacrificed
B
Saline
Elastase
Vehicle
MTX
Vehicle
MTX
C
Maximal diameter of abdominal aortas (mm)
2.0
1.5
1.0
0.5
0
*
*
Vehicle
MTX
Vehicle
MTX
Saline
Elastase
D
Saline
Elastase
Vehicle
MTX
Vehicle
MTX
400 μm
25 μm
E
Vehicle
MTX
Elastin degradation grade
4
3
2
1
0
*
*
Saline
Elastase
F
Vehicle
MTX
Saline
Elastase
25 μm

Here, we provided stronger evidence and drew our conclusion based on the analysis of the data network, which had the significance of guidance and prediction. Moreover, we found that MTX, which is widely used to treat autoimmune diseases, could prevent the formation and progression of AAA. However, it is unknown whether the mechanism of action of MTX in AAA is similar to its mechanism of action in RA; this question deserves further study. Aside from AAA, we also found that the most frequent category of neighbors to inflammation is neoplasms, and the most frequent category of neighbors to Huntington disease (HD) is immune system disease. As reported previously, inflammation is a hallmark of cancer [37], and innate immune activation is involved in the pathogenesis of HD [38]. These findings suggest that our algorithm is applicable to diseases other than AAA.

With the rapid growth of biomedical datasets, network medicine presents an excellent opportunity to investigate the mechanisms of complex diseases and develop new therapies; however, its application is still limited by the incompleteness of the available data and customized tools. In the current study, we introduced a new method, the Tanimoto coefficient, to measure disease similarity and construct a disease network to investigate novel disease associations. In contrast to methods used in previous studies, this method not only provides weight and direction information but also takes the influence of research imbalance into account. The findings in this study present an improved framework for the use of MRDN to address various questions in medicine. Besides, several important issues need to be addressed in the future. We noticed that many diseases in our dataset were associated with only a few miRNAs, and there were some diseases that were not linked to any diseases in the network, which may be due in part to the incompleteness of the current data. Additionally, current miRNA–disease association data do not contain organ distribution information, which would be useful for accurate representation of diseases, as miRNAs from different organs or tissues might be involved in different biological processes and play different roles in disease. In addition, miRNA expression information may not reflect all processes of a disease. So far, integrating multi-omics data into network medicine could also benefit similar analyses in the future.

Materials and methods

The human miRNA–disease association dataset

The human miRNA–disease association dataset was downloaded from the HMDD database (version 3.0) (http://www.cuilab.cn/hmdd/), which is a database of manually curated experimental evidence for associations between human miRNAs and diseases. In the HMDD, all associations are classified into six different categories: Circulation, Tissue, Genetics, Epigenetics, Target, and Other. Here, we extracted those associations with unambiguous tissue expression regulation information, that is, records with evidence code "tissue_expression_down" or "tissue_expression_up" in class "Tissue", for further analysis. Disease names were unified using MeSH, and miRNAs were assessed at the pre-miRNA level.

Calculation of miRNA-based disease similarity

We first defined each disease using a vector composed of the miRNAs associated with that disease. The value of each dimension represents the strength of the relationship between the disease and a particular miRNA. The quantitative strength of the relationship between disease i and miRNA j was calculated by the following formula:

$$w_{ij} = \sum_{k=1}^{R_{ij}} P_{ijk} \times \log\left(\frac{N}{n_j}\right) \quad (1)$$

where R_{ij} represents the number of records that link disease i and miRNA j, while P_{ijk} represents the direction of change in miRNA j in disease i in record k. If the expression level of miRNA j in disease i was up-regulated in record k, $P_{ijk} = 1$; inversely, if the expression level of miRNA j was down-regulated, $P_{ijk} = -1$. N is the total number of diseases in the curated dataset, and n_j is the number of diseases associated with miRNA j. As we hypothesize that miRNAs specifically associated with more diseases may contribute less to each disease, the penalty term $\log(N/n_j)$ was performed to decrease the weights of miRNAs with high disease spectrum width (DSW) and increase the weights of miRNAs with low DSW, in order to improve the discrimination and specificity among different diseases. As for the miRNA–disease pairs for which $R_{ij} = 0$, meaning that there are no available records mentioning the tissue expression regulation of miRNA j in disease i, their w_{ij} was set to 0. Then, each disease was described by a vector in the following form:

$$d_i = \left[w_{i1}, w_{i2}, \cdots, w_{ij}, \cdots, w_{iM}\right] \quad (2)$$

where M represents the number of all miRNAs in the curated dataset. Next, we used the Tanimoto coefficient to calculate the similarity between diseases. The similarity between disease x and disease y was calculated as follows:

$$S_{xy} = \frac{d_x \cdot d_y}{\|d_x\|^2 + \|d_y\|^2 - d_x \cdot d_y} \quad (3)$$

Figure 5 MTX attenuates the elastase-induced AAA formation

A. Administration scheme of MTX. 0.1% methylcellulose was applied as a vehicle control. **B.** and **C.** Representative *ex vivo* images of aortas (B) and quantification of maximal diameters of the infrarenal aortas (C) in saline- or elastase-induced mice treated with vehicle or MTX. *, $P < 0.05$ (two-way ANOVA followed by Tukey's test). **D.** and **E.** Representative images (D) and quantification of elastin Verhoeff-Van Gieson staining (E) in the cross-sections of infrarenal aortas in saline- or elastase-induced mice treated with vehicle or MTX. Scale bars, 400 μm and 25 μm. *, $P < 0.05$ (two-way ANOVA followed by Tukey's test). **F.** Representative immunofluorescence staining of macrophages ($CD68^+$, red) in infrarenal aortas. Scale bar, 25 μm. Saline + Vehicle, $n = 6$; Saline + MTX, $n = 6$; Elastase + Vehicle, $n = 6$; Elastase + MTX, $n = 6$. i.g., intragastric gavage; ANOVA, analysis of variance.

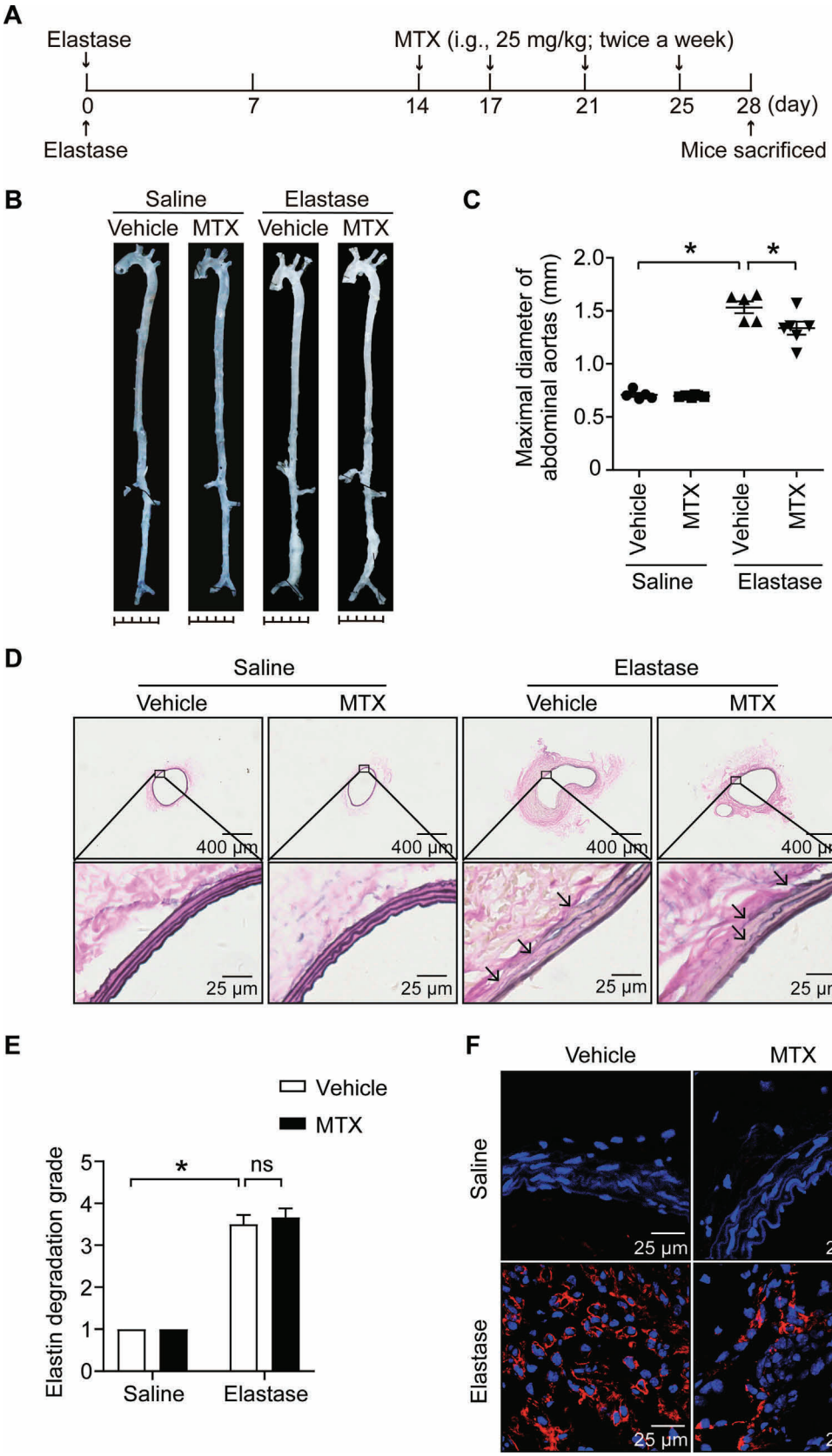
A
Elastase
MTX (i.g., 25 mg/kg; twice a week)
0
7
14
17
21
25
28 (day)
Elastase
Mice sacrificed
B
Saline
Elastase
Vehicle
MTX
Vehicle
MTX
C
Maximal diameter of abdominal aortas (mm)
2.0
1.5
1.0
0.5
0
*
*
Vehicle
MTX
Vehicle
MTX
Saline
Elastase
D
Saline
Elastase
Vehicle
MTX
Vehicle
MTX
400 μm
25 μm
E
Vehicle
MTX
Elastin degradation grade
5
4
3
2
1
0
*
ns
Saline
Elastase
F
Vehicle
MTX
Saline
Elastase
25 μm

There are two main methods to measure disease similarity: semantic similarity and vector-based similarity. The calculation of disease semantic similarity relies on a known disease classification system, which is not suitable for the discovery of new disease relationships. Calculation of vector-based disease similarity is based on the association data between disease and other factors such as genes, drugs, phenotypes, microbes, and miRNAs. A limitation of existing methods for evaluating miRNA-based disease similarity is that a disease is typically represented as a series of binary (present/absent) observations of miRNAs, lacking weights and directions. Using the cosine of two disease vectors as a similarity metric is the most straightforward way to overcome this problem. However, it tends to overestimate the connections between well-studied diseases and newly discovered diseases, in which situation the directions might be similar but the weights are different. The Tanimoto coefficient is an improved similarity calculation method that is derived from cosine similarity but also takes the norms of the two vectors into consideration. The greater the difference between the norms of two vectors, the smaller the Tanimoto coefficient is. Thus, in the present study, we use the Tanimoto coefficient as a similarity measurement to reduce the influence of research imbalances.

Construction of the MRDN

To construct the disease network, we calculated the pairwise disease similarities using the formula mentioned above. The Tanimoto similarity between diseases can range from -1 to 1. A similarity close to 1 indicates that the regulation directions of shared miRNAs tend to be the same, that is, the expression levels of miRNAs are both up-regulated or both down-regulated, whereas a similarity close to -1 indicates that the regulation directions of shared miRNAs tend to be opposite. A similarity equal to 0 means that there are no shared miRNAs between the two diseases. Then, we constructed the network of human diseases by linking every pair of diseases whose similarity has an absolute value above a chosen threshold (here, we set the threshold to 0.05 based on network topology). In visual depictions of the network, similar diseases are linked by a solid orange line or a dashed blue line if their similarity is positive or negative, respectively. The layouts of the MRDN were generated by manual arrangement using Cytoscape, and the network parameters were calculated using the Python package NetworkX.

Reagents

Type I porcine pancreatic elastase (E1250; Catalog No. SLBV9311) and MTX (Catalog No. A6770) were purchased from Sigma-Aldrich (St Louis, MO). Methylcellulose (Catalog No. STUM87231) were purchased from Solarbio Life Sciences (Beijing, China). Rat antimouse CD68 (Catalog No. MCA1957) was purchased from AbD Serotec (Kidlington, UK). Alexa Fluor 555 anti-mouse IgG secondary antibody (Catalog No. 1685557) was purchased from Life Technologies (San Diego, CA). Tissue-Tek O.C.T. Compound (Catalog No. 4583) was purchased from Sakura (Torrance, CA). Verhoeff-Van Gieson Stain Kit (Catalog No. BSBA-4083B) was purchased from BASO (Zhuhai, China).

Elastase-induced AAA model

C57BL/6J mice (ten-week-old male) were purchased from Vital River (Beijing, China) and used for an elastase-induced AAA model. Compared with female mice, male mice are more susceptible to AAA [39–41], so male mice were selected in the experiment. Elastase-induced AAA was performed as described in previous studies [42,43]. In brief, each mouse was anesthetized, and its abdominal cavity was opened to expose the aorta. The infrarenal aorta was separated, coated with sterile cotton, and incubated with 30 μl of elastase (44.1 IU/ml) for 40 min. Then, before suturing, the cotton was removed and the abdominal cavity was irrigated with 0.9% sterile NaCl.

To measure the diameter of AAA, the mice were sacrificed and then perfused with phosphate-buffered saline (PBS) and fixed with 4% paraformaldehyde. The aortas from the aortic root to the iliac bifurcation were isolated and fixed on a wax plate, and images were captured of the aortas along with a ruler for scale. The maximal diameters of the infrarenal aortas were used as quantitative data and subjected to statistical analysis.

Design of MTX and HCQ experiments

The mice were randomly divided into an elastase-induced model group (model group) and an elastase-induced model group treated with MTX (MTX group). To explore whether MTX treatment alleviated the occurrence of AAA, the mice in the model group were administered 200 μl 0.1% methylcellulose (i.g., twice a week), and the mice in the MTX group received 200 μl MTX (i.g., 15 mg/kg; twice a week) from the day of elastase-induced AAA and lasted for 14 days. Next, to explore the therapeutic effects of MTX on AAA, 200 μl 0.1% methylcellulose (i.g., twice a week) and MTX (i.g., 15 mg/kg; twice a week) were given to the mice in the model group and MTX group, respectively, starting 14 days after surgery and continuing for 14 days.

In the same way, the mice were randomly divided into an elastase-induced model group (model group) and an elastase-induced model group treated with HCQ (HCQ group). The mice in the model group were administered 200 μl 0.9% NaCl

Figure 6 MTX inhibits the elastase-induced AAA development

A. Administration scheme of MTX. 0.1% methylcellulose was applied as vehicle control. **B.** and **C.** Representative *ex vivo* images of aortas (B) and quantification of maximal diameters of the infrarenal aortas (C) in saline- or elastase-induced mice treated with vehicle or MTX. *, $P < 0.0$ (two-way ANOVA followed by Tukey's test). **D.** and **E.** Representative images (D) and quantification of elastin Verhoeff-Van Gieson staining (E) in the cross-sections of infrarenal aortas in saline- or elastase-induced mice treated with vehicle or MTX. Scale bars, 400 μm and 25 μm. *, $P < 0.05$; ns, no significance (two-way ANOVA followed by Tukey's test). **F.** Representative immunofluorescence staining of macrophages ($CD68^+$, red) in infrarenal aortas. Scale bar, 25 μm. Saline + Vehicle, $n = 5$; Saline + MTX, $n = 6$; Elastase + Vehicle, $n = 5$; Elastase + MTX, $n = 6$.

(i.e., daily), and the mice in the HCQ group received 200 μl HCQ (i.e., 100 mg/kg; daily), starting on the same day as elastase-induced AAA and continuing for 14 days.

Elastin staining

Infrarenal aortas were embedded in Tissue-Tek O.C.T. Compound, and then 7-μm-thick frozen sections were cut on slides at 70-μm intervals. Sections from each mouse were subjected to staining of elastin using a Verhoeff-Van Gieson Stain Kit. Elastin degradation was graded by two blinded individuals on a scale of 1–4, where 1 represented < 25% degradation, 2 represented 25%–50% degradation, 3 represented 50%–75% degradation, and 4 represented > 75% degradation.

Immunofluorescence staining

Cross-sections of infrarenal aortas were incubated with rat anti-mouse CD68 antibodies (1:200 dilution, 5 μg/ml) at 4 °C overnight, followed by incubation with Alexa Fluor 555 anti-mouse IgG secondary antibody (1:1000 dilution, 2 μg/ml) at 37 °C for 1 h, while mouse IgG of equal concentration was used at the primary antibody stage as a negative control. Nuclei were counterstained using 2-(4-Amidinophenyl)-6-indolecarbamidine dihydrochloride (DAPI) (1:1000; Invitrogen, Waltham, MA).

Statistical analysis

All the results are presented as the mean ± standard error of the mean (SEM). GraphPad Prism 6.0 (GraphPad Software, San Diego) was used for statistical analyses. For the statistical comparison, we first assessed whether the data conformed to the normal distribution. If the variances were similar, normally distributed data were analyzed using Student's *t*-test for two-group comparisons and analysis of variance (ANOVA) for comparisons among more than two groups. Nonparametric tests were used for the data that were not normally distributed. In all cases, statistical significance was concluded if the two-tailed probability was < 0.05. The details of the statistical analysis are presented in the corresponding figure legends.

Ethics statement

All animal studies and experimental procedures followed the guidelines of the Animal Care and Use Committee of Peking University, China. The animal study was reviewed and approved by Laboratory Animal Welfare Ethics Branch, Biomedical Ethics Committee of Peking University (Approval No. LA2019126).

Code availability

Our network analysis is based on Python 3 and R. The codes used for data processing and analyses have been submitted to BioCode at the National Genomics Data Center, Beijing Institute of Genomics, Chinese Academy of Sciences / China National Center for Bioinformation (BioCode: BT007302), which are publicly available at https://ngdc.cncb.ac.cn/biocode/tools/BT007302.

Competing interests

The authors have declared no competing interests.

CRediT authorship contribution statement

Yicong Shen: Methodology, Formal analysis, Visualization, Data curation, Writing – original draft. **Yuanxu Gao:** Methodology, Formal analysis, Visualization, Data curation, Writing – original draft. **Jiangcheng Shi:** Data curation. **Zhou Huang:** Data curation. **Rongbo Dai:** Methodology. **Yi Fu:** Writing – review & editing, Supervision. **Yuan Zhou:** Writing – review & editing, Supervision. **Wei Kong:** Conceptualization, Writing – original draft, Writing – review & editing, Supervision. **Qinghua Cui:** Conceptualization, Writing – original draft, Writing – review & editing, Supervision. All authors have read and approved the final manuscript.

Acknowledgments

This work has been supported by the grants from the PKU-Baidu Fund (Grant No. 2019BD014) and the National Natural Science Foundation of China (Grant Nos. 81970440 and 62025102 to Qinghua Cui; Grant Nos. 31930056, 81730010, and 91539203 to Wei Kong).

Supplementary material

Supplementary data to this article can be found online at https://doi.org/10.1016/j.gpb.2022.08.002.

ORCID

ORCID 0000-0002-8526-2338 (Yicong Shen)
ORCID 0000-0001-5314-0195 (Yuanxu Gao)
ORCID 0000-0001-9934-4556 (Jiangcheng Shi)
ORCID 0000-0001-6369-5565 (Zhou Huang)
ORCID 0000-0001-9259-363X (Rongbo Dai)
ORCID 0000-0002-8832-9331 (Yi Fu)
ORCID 0000-0001-5685-066X (Yuan Zhou)
ORCID 0000-0001-6720-6810 (Wei Kong)
ORCID 0000-0003-3018-5221 (Qinghua Cui)

References

[1] Nordon IM, Hinchliffe RJ, Loftus IM, Thompson MM. Pathophysiology and epidemiology of abdominal aortic aneurysms. Nat Rev Cardiol 2011;8:92–102.
[2] Golledge J. Abdominal aortic aneurysm: update on pathogenesis and medical treatments. Nat Rev Cardiol 2019;16:225–42.
[3] Sakalihasan N, Limet R, Defawe OD. Abdominal aortic aneurysm. Lancet 2005;365:1577–89.
[4] Kent KC. Abdominal aortic aneurysms. N Engl J Med 2014;371:2101–8.

[5] Sampson UKA, Norman PE, Fowkes FGR, Aboyans V, Song Y, Harrell Jr FE, et al. Estimation of global and regional incidence and prevalence of abdominal aortic aneurysms 1990 to 2010. Glob Heart 2014;9:159–70.
[6] GBD 2013 Mortality and Causes of Death Collaborators. Global, regional, and national age-sex specific all-cause and cause-specific mortality for 240 causes of death, 1990–2013: a systematic analysis for the Global Burden of Disease Study 2013. Lancet 2015;385:117–71.
[7] Golledge J, Norman PE. Current status of medical management for abdominal aortic aneurysm. Atherosclerosis 2011;217:57–63.
[8] Pushpakom S, Iorio F, Eyers PA, Escott KJ, Hopper S, Wells A, et al. Drug repurposing: progress, challenges and recommendations. Nat Rev Drug Discov 2019;18:41–58.
[9] Hodos RA, Kidd BA, Shameer K, Readhead BP, Dudley JT. *In silico* methods for drug repurposing and pharmacology. Wiley Interdiscip Rev Syst Biol Med 2016;8:186–210.
[10] Cha Y, Erez T, Reynolds IJ, Kumar D, Ross J, Koytiger G, et al. Drug repurposing from the perspective of pharmaceutical companies. Br J Pharmacol 2018;175:168–80.
[11] Demchak B, Kreisberg JF, Bass JIF. Theory and application of network biology toward precision medicine. J Mol Biol 2018;430:2873–4.
[12] Sonawane AR, Weiss ST, Glass K, Sharma A. Network medicine in the age of biomedical big data. Front Genet 2019;10:294.
[13] Pai S, Bader GD. Patient similarity networks for precision medicine. J Mol Biol 2018;430:2924–38.
[14] Pai S, Hui S, Isserlin R, Shah MA, Kaka H, Bader GD. netDx: interpretable patient classification using integrated patient similarity networks. Mol Syst Biol 2019;15:e8497.
[15] Li L, Cheng WY, Glicksberg BS, Gottesman O, Tamler R, Chen R, et al. Identification of type 2 diabetes subgroups through topological analysis of patient similarity. Sci Transl Med 2015;7:311ra174.
[16] Ma W, Zhang L, Zeng P, Huang C, Li J, Geng B, et al. An analysis of human microbe–disease associations. Brief Bioinform 2017;18:85–97.
[17] Zhou X, Menche J, Barabasi AL, Sharma A. Human symptoms-disease network. Nat Commun 2014;5:4212.
[18] Rupaimoole R, Slack FJ. MicroRNA therapeutics: towards a new era for the management of cancer and other diseases. Nat Rev Drug Discov 2017;16:203–22.
[19] Huang Z, Shi J, Gao Y, Cui C, Zhang S, Li J, et al. HMDD v3.0: a database for experimentally supported human microRNA–disease associations. Nucleic Acids Res 2019;47:D1013–7.
[20] Hu JX, Thomas CE, Brunak S. Network biology concepts in complex disease comorbidities. Nat Rev Genet 2016;17:615–29.
[21] Menche J, Sharma A, Kitsak M, Ghiassian SD, Vidal M, Loscalzo J, et al. Uncovering disease-disease relationships through the incomplete interactome. Science 2015;347:1257601.
[22] Barabasi AL, Gulbahce N, Loscalzo J. Network medicine: a network-based approach to human disease. Nat Rev Genet 2011;12:56–68.
[23] Goh KI, Cusick ME, Valle D, Childs B, Vidal M, Barabasi AL. The human disease network. Proc Natl Acad Sci U S A 2007;104:8685–90.
[24] Lu M, Zhang Q, Deng M, Miao J, Guo Y, Gao W, et al. An analysis of human microRNA and disease associations. PLoS One 2008;3:e3420.
[25] Sperling AS, Gibson CJ, Ebert BL. The genetics of myelodysplastic syndrome: from clonal haematopoiesis to secondary leukaemia. Nat Rev Cancer 2017;17:5–19.
[26] Marian AJ, Braunwald E. Hypertrophic cardiomyopathy: genetics, pathogenesis, clinical manifestations, diagnosis, and therapy. Circ Res 2017;121:749–70.
[27] Wang J, Gu BJ, Masters CL, Wang YJ. A systemic view of Alzheimer disease - insights from amyloid-beta metabolism beyond the brain. Nat Rev Neurol 2017;13:612–23.
[28] Milo R, Shen-Orr S, Itzkovitz S, Kashtan N, Chklovskii D, Alon U. Network motifs: simple building blocks of complex networks. Science 2002;298:824–7.
[29] Tilson MD. Decline of the atherogenic theory of the etiology of the abdominal aortic aneurysm and rise of the autoimmune hypothesis. J Vasc Surg 2016;64:1523–5.
[30] Singh JA, Saag KG, Bridges Jr SL, Akl EA, Bannuru RR, Sullivan MC, et al. 2015 American College of Rheumatology guideline for the treatment of rheumatoid arthritis. Arthritis Care Res (Hoboken) 2016;68:1–25.
[31] Gordon C, Amissah-Arthur MB, Gayed M, Brown S, Bruce IN, D'Cruz D, et al. The British Society for Rheumatology guideline for the management of systemic lupus erythematosus in adults. Rheumatology (Oxford) 2018;57:e1–45.
[32] Pigott E, DuHadaway JB, Muller AJ, Gilmour S, Prendergast GC, Mandik-Nayak L. 1-methyl-tryptophan synergizes with methotrexate to alleviate arthritis in a mouse model of arthritis. Autoimmunity 2014;47:409–18.
[33] An N, Chen Y, Wang C, Yang C, Wu ZH, Xue J, et al. Chloroquine autophagic inhibition rebalances Th17/Treg-mediated immunity and ameliorates systemic lupus erythematosus. Cell Physiol Biochem 2017;44:412–22.
[34] Bracken CP, Scott HS, Goodall GJ. A network-biology perspective of microRNA function and dysfunction in cancer. Nat Rev Genet 2016;17:719–32.
[35] Hirose H, Tilson MD. Abdominal aortic aneurysm as an autoimmune disease. Ann N Y Acad Sci 2001;947:416–8.
[36] Hirose H, Tilson MD. Negative genetic risk factor for abdominal aortic aneurysm: HLA-DQ3, a Japanese study. J Vasc Surg 1999;30:959–60.
[37] Hanahan D, Weinberg RA. Hallmarks of cancer: the next generation. Cell 2011;144:646–74.
[38] Lee H, Fenster RJ, Pineda SS, Gibbs WS, Mohammadi S, Davila-Velderrain J, et al. Cell type-specific transcriptomics reveals that mutant huntingtin leads to mitochondrial RNA release and neuronal innate immune activation. Neuron 2020;107:891–908.
[39] Ailawadi G, Eliason JL, Roelofs KJ, Sinha I, Hannawa KK, Kaldjian EP, et al. Gender differences in experimental aortic aneurysm formation. Arterioscler Thromb Vasc Biol 2004;24:2116–22.
[40] Alsiraj Y, Thatcher SE, Charnigo R, Chen K, Blalock E, Daugherty A, et al. Female mice with an XY sex chromosome complement develop severe angiotensin II-induced abdominal aortic aneurysms. Circulation 2017;135:379–91.
[41] Robinet P, Milewicz DM, Cassis LA, Leeper NJ, Lu HS, Smith JD. Consideration of sex differences in design and reporting of experimental arterial pathology studies-statement from ATVB council. Arterioscler Thromb Vasc Biol 2018;38:292–303.
[42] He L, Fu Y, Deng J, Shen Y, Wang Y, Yu F, et al. Deficiency of FAM3D (family with sequence similarity 3, member d), a novel chemokine, attenuates neutrophil recruitment and ameliorates abdominal aortic aneurysm development. Arterioscler Thromb Vasc Biol 2018;38:1616–31.
[43] Li T, Yu B, Liu Z, Li J, Ma M, Wang Y, et al. Homocysteine directly interacts and activates the angiotensin II type I receptor to aggravate vascular injury. Nat Commun 2018;9:11.